

# Next-Generation Fibre-Reinforced Lightweight Structures for Additive Manufacturing

J. Plocher and A. Panesar

*Department of Aeronautics, Imperial College London, SW7 2AZ, UK*

*Emails: [janos.plocher16@imperial.ac.uk](mailto:janos.plocher16@imperial.ac.uk); [a.panesar@imperial.ac.uk](mailto:a.panesar@imperial.ac.uk)*

## **Abstract**

In an attempt to realise next-generation lightweight parts and to fully utilize the inherent design freedom of AM, we propose a topology optimization based design procedure that includes the anisotropic considerations for continuous fibre printing of variable stiffness composites. In this paper, we aim to improve the normalized compliance of a beam in a three-point bending scenario, using a skeletal reinforcement for a topology in which the change in fibre orientation is derived from the medial axis information. FDM with a dual-nozzle system printing nylon and carbon fibre filaments were utilized for fabrication. The toolpath i.e. reinforcement strategy available from the commercial software Eiger® was chosen to imitate the proposed strategy. The numerical investigation is complemented with experimental tests and a general benchmarking is conducted using standard pedants. The results have shown improved specific flexural stiffness for samples with skeletal reinforcement. The skeletal information is therefore considered as important tool for the retrieval of fibre angles which align with the principle stresses and therefore allow for a more efficient fibre placement in AM parts for future lightweight end-use parts.

## **1 Introduction**

Design and structural optimization for additive manufacturing is gaining immense traction in the research community and are key stones towards next generation manufacturing and lightweight structures [1–3]. Topology optimization (TO), a numerical tool which centres around the redistribution of material in a given design space based on the applied boundary and loading conditions, has meanwhile established itself as means of structural optimization for additively manufactured parts. In pursuit of improved structural performance and functionality in additively manufactured parts, we experience increased efforts in the research community to promote AM of composites. The authors believe, that the effective combination of both methods in AM will enable next generation light and polymer-based structures as well as generally providing a wider range of application as end-use parts. For the successful implementation however, design for AM (DfAM) will be playing pivotal role.

DfAM becomes particularly important for the successful manufacturing of the complex freeform geometries created by TO. From one of the first definitions by Rosen [4] focusing on the AM-specific criteria affecting the performance (shape, microstructure, etc.) to the most recent heuristic definition and framework by Kumke et al. [5], which includes both design rules related to the manufacturing constraints and the vast design potential of AM.

### ***1.1 Medial Axis Transformation (MAT) for structural enhancement***

MAT i.e. the extraction of the skeleton of an arbitrary shape has previously found application in both AM [6–8] and TO [9]. More recently however, studies have shown the great benefit of using it across the two fields to implement for instance manufacturing constraints in a level set TO [10] or circuitry into AM parts for enhanced functionality while preserving the structural performance [11]. In the context of DfAM, the MAT has further proven as viable solution for a gap-free toolpath generation [6,7]. As such it offers the possibility to adapt infills for fibre reinforced AM (FRAM).

### ***1.2 Fibre-reinforced Additive Manufacturing (FRAM)***

The majority of research into AM of composites employs FDM with either short or continuous fibre-reinforced filaments [12–17], although magnetically assisted STL [18], electrically supported VAT [19] and jetting [20] were also used for this purpose. For further reading, Quan et al. [21] supply a summary of fibre reinforced AM with different processes. Generally FRAM can be divided into short fibre-reinforced AM (S-FRAM) and continuous fibre-reinforced AM (C-FRAM). With the increasing supply of hardware from companies like Markforged Inc. [22], Arevo Inc. [23] or Continuous Composites [24], this work focuses mainly on C-FRAM, as it provides maximum structural performance and the greatest potential for lightweight structures from AM.

### ***1.3 Topology Optimization with Anisotropic Considerations for Additive Manufacturing***

In polymer-based AM of composites, we can differentiate between the mixture of different polymers and the reinforcement of a polymers with a non-polymeric constituent. The former has been particularly attractive for the level set TO, as research has been conducted to investigate the effect of using two materials with dissimilar properties on the topology [25,26] and another work by Zhu et al. [27] has employed the method in conjunction with microstructures for printable structures. Subject of interest in this work is however FRAM which is a field of research gaining momentum as is increasingly brought in context with TO [28–31]. Most recently, through the introduction of CFAO (Continuous Fibre Angle Optimization) i.e. TO with fibre reinforcement for 2D structures by Høglund et al. [29,32] and its further improvement by Jiang et al. [30,31]. Besides the density, the fibre angle represents hereby the second design variable for the TO, which is included into the elastic constitutive matrix. The adjoint method, used for the sensitivity analysis in their work [32] might generally be an effective way to realize TO with fibre angle optimization or any other constraints related to e.g DfAM.

### ***1.4 Scope of this paper***

This work aims to demonstrate how the medial axis transformation (MAT) on topologically optimized structures can function as a tool to introduce anisotropy for additively manufactured parts. Besides a theoretical simulation of a topologically optimized structure enhanced by the skeletal information, this paper intends to illustrate further methodologies that can be obtained from

TO-based MAT for the realization of light, anisotropic structures with minimized compliance. With the aid and within the capabilities of current commercially available printers, an indication of correspondingly achievable mechanical properties is presented. In this context additional workflows describing ways to obtain physical specimens that resemble the proposed designs are disclosed.

## **2 Methodology – Approaches Considering Anisotropy in Topology Optimization**

Three different approaches to obtain lightweight structures for AM with anisotropic considerations are proposed and detailed in Figure 1. TO and MAT represent the core concepts while aspects of DfAM are considered on the premise of an implementation with C-FRAM. The overarching methodology for all three approaches can be clustered into the following 4 consecutive process steps:

- **Isotropic TO** – Solid Isotropic Material with Penalization (SIMP) is conducted upon a given design domain and boundary conditions. A pre-selected criteria (e.g. premature termination of iterative process) determines whether to proceed or not. Finally a greyscale image of the topology is obtained.
- **MAT** – A binarization of the greyscale density matrix is a prerequisite for the subsequent MAT. Information on the end-point, branch-points, links, etc. of the resultant skeleton can then be used for further updates such as segmentation, dilation, etc. This skeletonisation provides beneficial information (slope of links, nodal connectivity, etc.) for the implementation of fibre reinforcement into additively manufactured parts.
- **Selection of approach** – For the incorporation of anisotropy we propose the following three approaches shown in Figure 1, which will be described in more detail in the subsequent sections.
- **Update scheme** – Each individual approach includes some sort of update scheme which post-processes the MAT information. The individual schemes will be described in the following and will be illustrated in workflows.

Methods pertinent to realisation of the approaches discussed in Figure 1 are detailed in the subsections below.

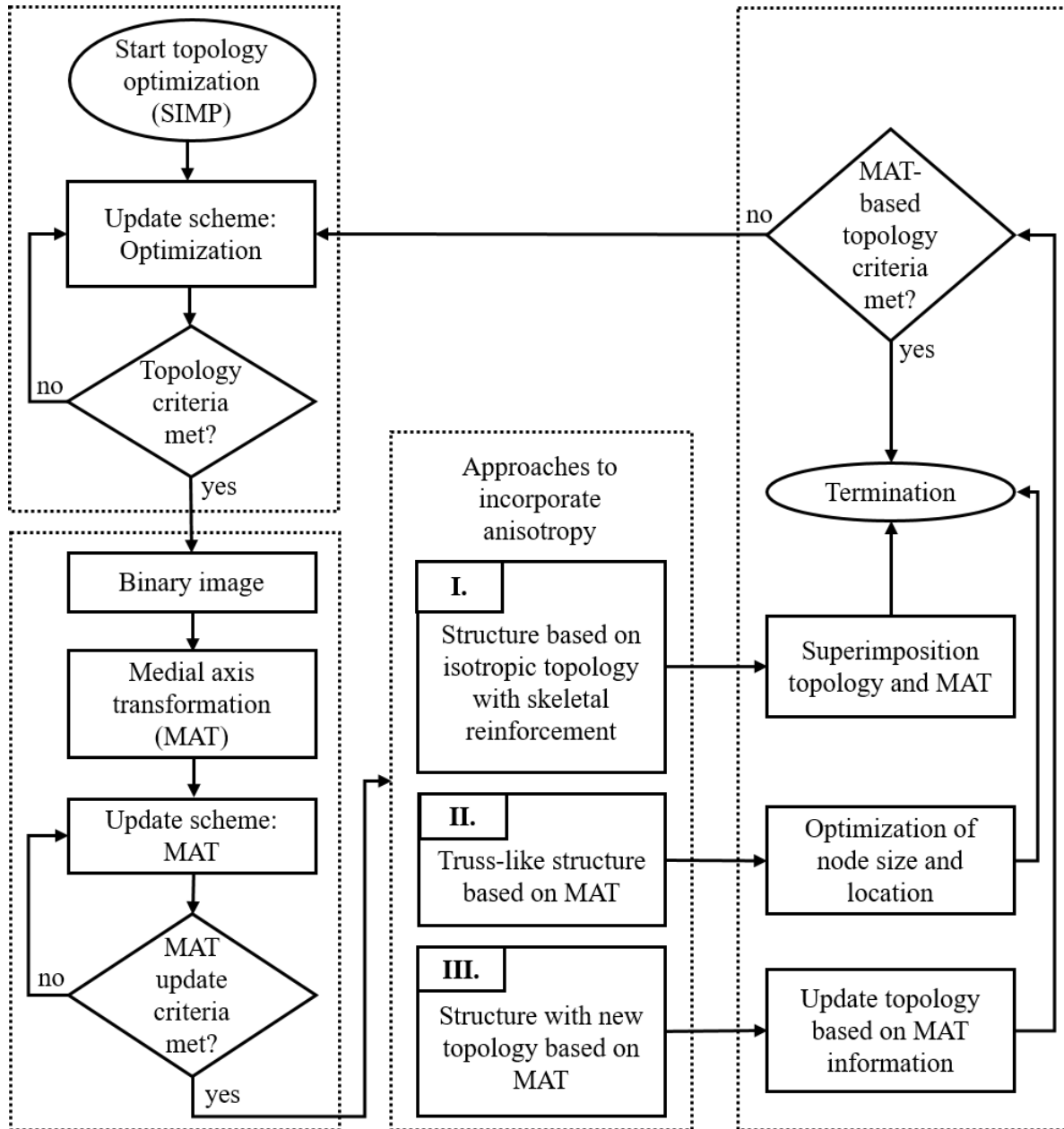


Figure 1: Flowchart of the presented methodology.

## 2.1 Solid Isotropic Material with Penalization (SIMP)

**Approach I. – Isotropic topology with skeletal reinforcement.** In this work, a beam under Three-Point Bending (3PB) was considered for the optimization. The SIMP method was utilized in pursuit of minimizing compliance (increased stiffness). The loading scenario is based on the ASTM D7264 /D7264M – 15 [33] standard, however alterations were made to the aspect ratio of the specimen and the roller diameters. The former was reduced to 4:1 in order to ensure good comparability with the common MBB-beam examples in the field of TO and the latter was

increased to mitigate the indentation of the rather soft AM-parts. Following the Matlab implementation of the density-based SIMP method of previous works [34–36], we obtained the two-dimensional TO solution with 0.5 volume fraction for isotropic material using a penalization factor of 3 and a filter size of 2 (see Figure 2). Subsequently, the greyscale image was transformed into a binary image based on a threshold value of 0.5 to enable the medial axis transformation.

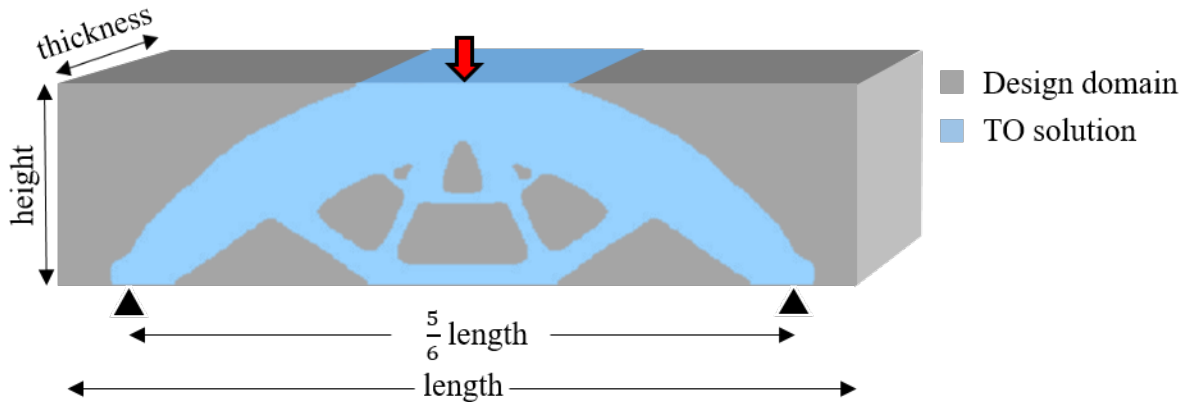


Figure 2: Initial design domain for the 3PB with 4:1 ratio of length to height as well as the final binarized TO solution obtained using SIMP.

**Approach II. – Truss-like structure based on MAT.** Similarly, the SIMP method was also employed for the truss approach, however, since it only serves as a feasibility study for a FEA in this work, the authors chose the classical cantilever example with an aspect ratio of 5:3 i.e a total of 1500 pixels. Hereby a volume fraction of 0.55 was applied and the resultant matrix was subsequently binarized.

## 2.2 Medial Axis Transformation (MAT)

A skeletonisation i.e. MAT of the TO solution represents the starting point for the three proposed methodologies. The method is based on the thinning algorithm introduced by Kerschnitzki et al. [37] and builds upon the work of Panesar et al. [8], however the computational efficiency of the MAT was improved in this work by utilizing the in-built Matlab function *bwmorph*, while still obtaining the skeletal information from the original code. Individual links were then further discretized using a step-size of 5 and a threshold angle of  $12^\circ$  to create sub-links. This segmentation is vital for the FEA, since it allows for a more representative assignment of fibre angles (for individual elements) based on the local tangent values.

**Approach I. – Isotropic topology with skeletal reinforcement.** For this method (see Figure 3) each newly formed sub-link is radially dilated based on the minimum distance between any point of a link and the eroded perimeter of the TO solution (see Figure 2), which is inspired by the routing strategies for AM introduced in [8]. The erosion ensures that at least a layer of pure matrix is maintained on the perimeter so that the fibre domain (dilated skeleton) is entirely encapsulated. In order to ensure a reinforcement of very small struts in the topology (see Figure 4), some skeletal

elements were allowed to coincide with the elements of the perimeter. Slopes between the end-nodes of each link served as principle fibre angle. The corresponding elements of each sub-link were subsequently assigned this angle (see Figure 4). The angle of the overlapping elements was updated by the consecutive sub-link adjoining at the rightmost node of the previous sub-link.

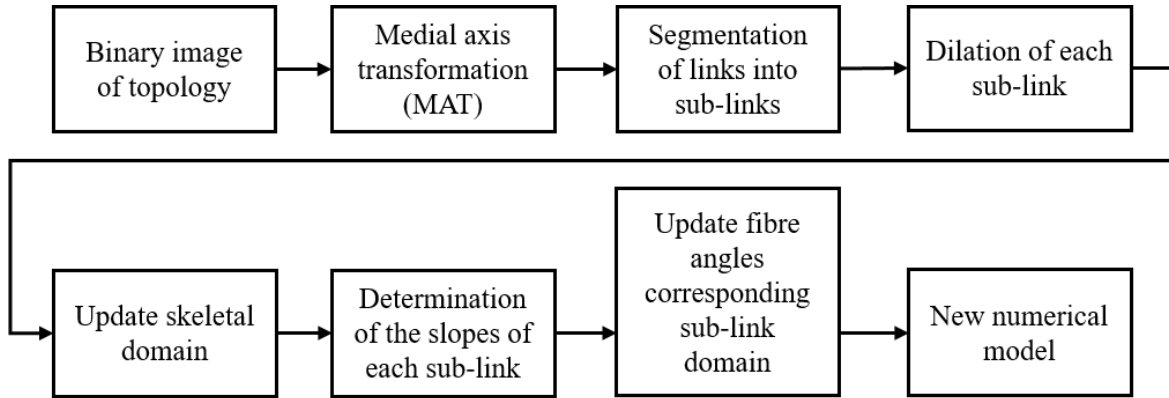


Figure 3: Workflow describing the obtainment of an isotropic topology with a skeletal reinforcement (approach I.).

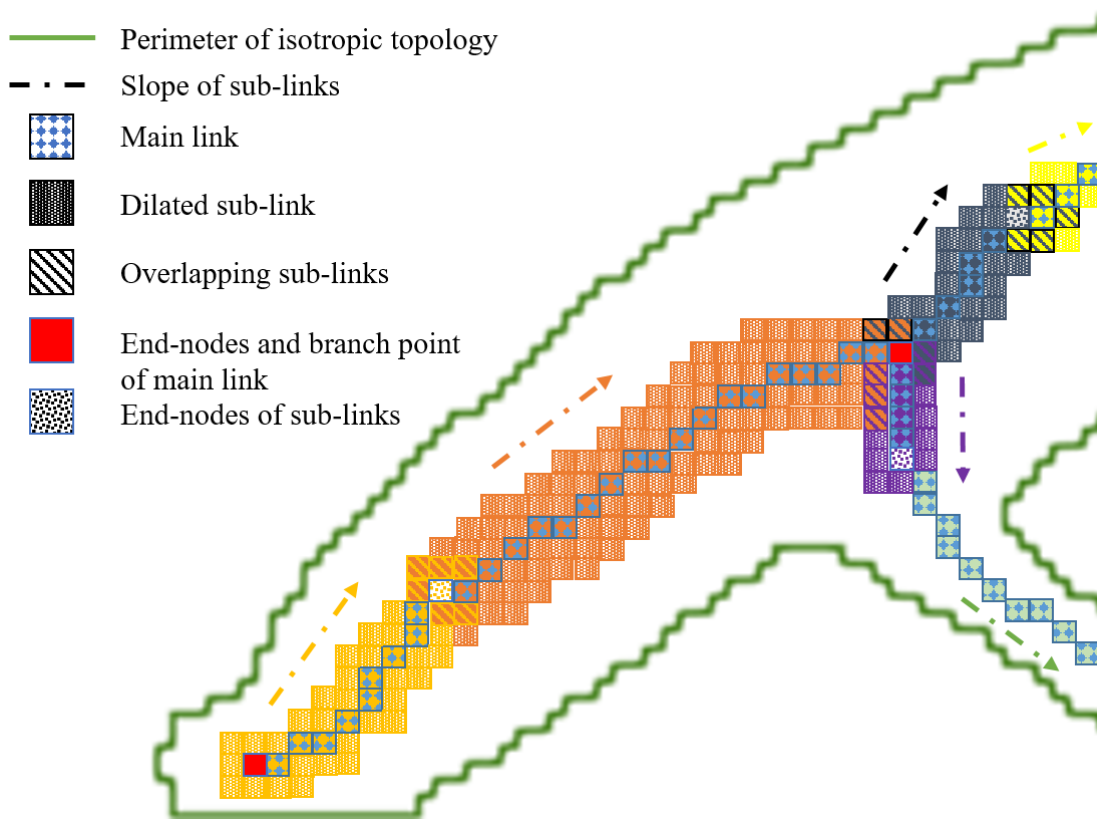


Figure 4: Schematic drawing explaining the concept behind the segmentation, dilation and fibre angle determination and assignment.

**Approach II. – Truss-like structure based on MAT.** Alternatively, the MAT information can be utilized to create an optimized truss-like structure, which can serve as a means for fabrication with anisotropic material. Depending on how detailed the topology shall be represented, major nodes or sub-link nodes can be connected using beam or rod elements. A nodal sizing optimization and subsequent perturbation can be realized using a sensitivity analysis or a genetic algorithm (GA). A weight fraction constraint can ensure that the same amount of material is employed in the optimized truss compared to the topology it was derived from and may serve as performance indicator.

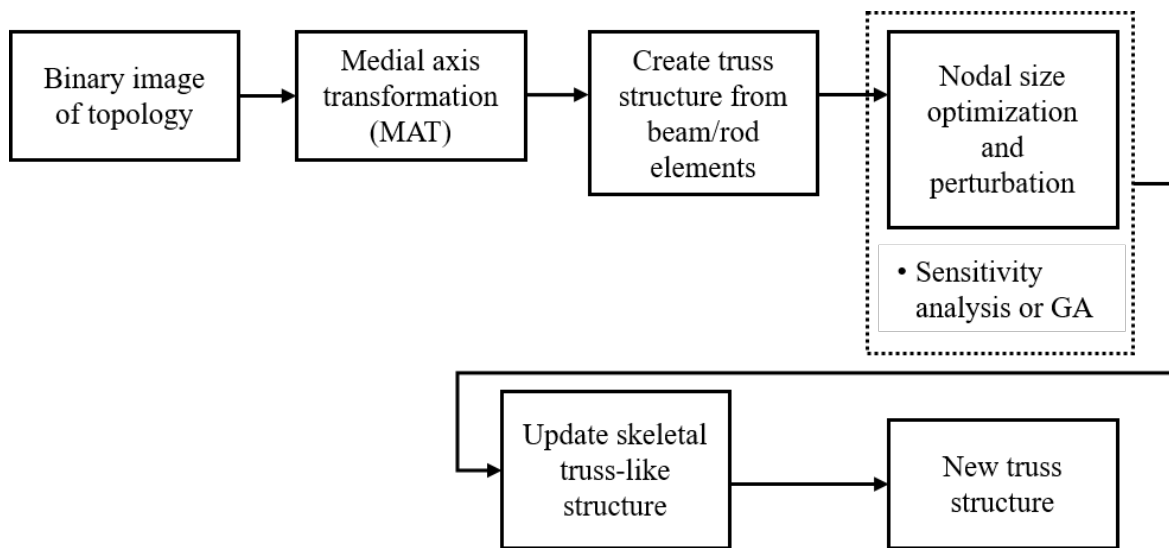


Figure 5: Workflow describing the obtainment of a truss-like structure based on MAT of an isotropic topologically optimized structure (approach II.).

**Approach III. – Topology updated with MAT information.** Although not further discussed in this work, the authors would like to present the idea of altering the topology based on the MAT information. Instead of a solution for an anisotropic reinforcement for an optimized topology (approach I. & II.), this could open up a way to realize an optimized topology with anisotropic considerations, which will be the subject of investigation in future work.

### 2.3 Finite Element Analysis (FEA)

FEA was conducted in parts within Matlab [38] and the CAE software Abaqus [39]. More precisely, FEA for the isotropic TO (step 1 in of the flowchart illustrated in Figure 1) was performed in Matlab, whereas Abaqus was used in analysing structures with anisotropic reinforcements. Linear static analyses were conducted for both approaches.

**Approach I. – Isotropic topology with skeletal reinforcement.** The density matrices of the TO solution and the dilated skeleton were represented as hexahedral elements in order to assign directional material properties to individual elements. In order to ensure that a minimum of 3 elements represent the thinnest member of the topology, the domain size was chosen as 400 elements (length) by 100 elements (height). Since the physical specimens were produced by the *Mark 2* printer (*Markforged, Inc.*), the theoretical material properties supplied by the manufacturer [40] were utilized. In order to comply with the larger loading rollers used and the indentation of the material at the surface, concentrated forces were applied as shown in Figure 6 (1 % of total area), whereby the load was linearly reduced from the mid-node towards the outermost nodes to total a force of 1N.

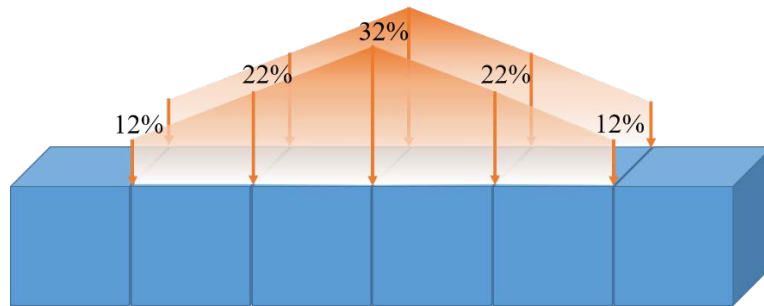


Figure 6: Linearly distributed load totaling to 1N used in the FEA to resemble loading in the 3PB test.

**Approach II. – Truss-like structure based on MAT.** The truss structure is represented by 2D beam elements with circular cross-section connected by the skeletal nodes. Both nodal size optimization and nodal perturbation were conducted using GA subject to minimal global strain energy. In the former case this was normalized by the area in order to retain comparability with the initial topology.

### 3 Methodology – From Design to Print

#### *Closed Source Implementation*

**Approach I. – Isotropic topology with skeletal reinforcement.** In an attempt to verify the primary methodology experimentally, *Markforged's* continuous fibre printer *Mark v 2* was employed. As illustrated by the workflow in Figure 7, a stl-file was created from the density matrix and uploaded to the corresponding enterprise software *Eiger*® [41], where the part, material and reinforcement setting were selected. This workflow is also applicable to the MAT-based truss structure, however was not implemented in this work. Each specimen was printed using 2 wall layers as well as roof and bottom layers. Within the capabilities of the *Eiger*® software, we have chosen to reinforce the topologically optimized samples with a concentric reinforcement in order to imitate the skeletal reinforcement proposed in approach I as close as possible.

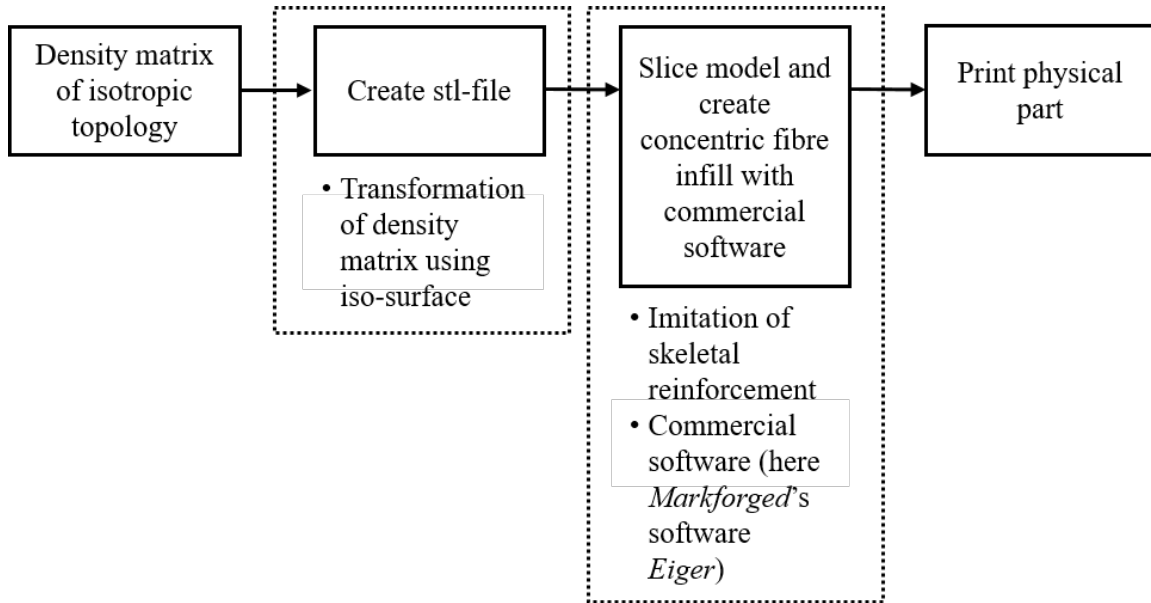


Figure 7: Workflow illustrating the steps required to obtain specimens that imitate the skeletal reinforcement described in the third methodology (approach I.) using the commercial software and printer of *Markforged Inc.*

For comparison specimens representing the entire domain (160mm x 40mm x 15mm) were also printed with pure matrix, quasi-isotropic (QI) layup and as benchmark with an uni-directional (UD) layup. Table 1 summarizes the different specimens tested in 3PB for this study and Figure 8 illustrates the build direction and reinforcement strategies i.e. fibre paths chosen for all specimens.

Table 1: Specimen specifications and corresponding designations for the mechanical testing.

Specimen type	Matrix material	Reinforcement	Abbreviation
Topologically optimized structure	Nylon	n.a.	N
	Nylon + Continuous CF	Concentric	CFR
	Nylon + Short CF	n.a.	SFR
	Nylon + Continuous and short CF	Concentric	S/C-FR
Reference structure (design domain)	Nylon	n.a.	Nref
	Nylon + Continuous CF	UD	CFRrefUD
	Nylon + Continuous CF	QI	CFRrefQI
	Nylon + Short CF	n.a.	SFRref
	Nylon + Continuous and short CF	UD	S/C-FRrefUD
	Nylon + Continuous and short CF	QI	S/C-FRrefQI

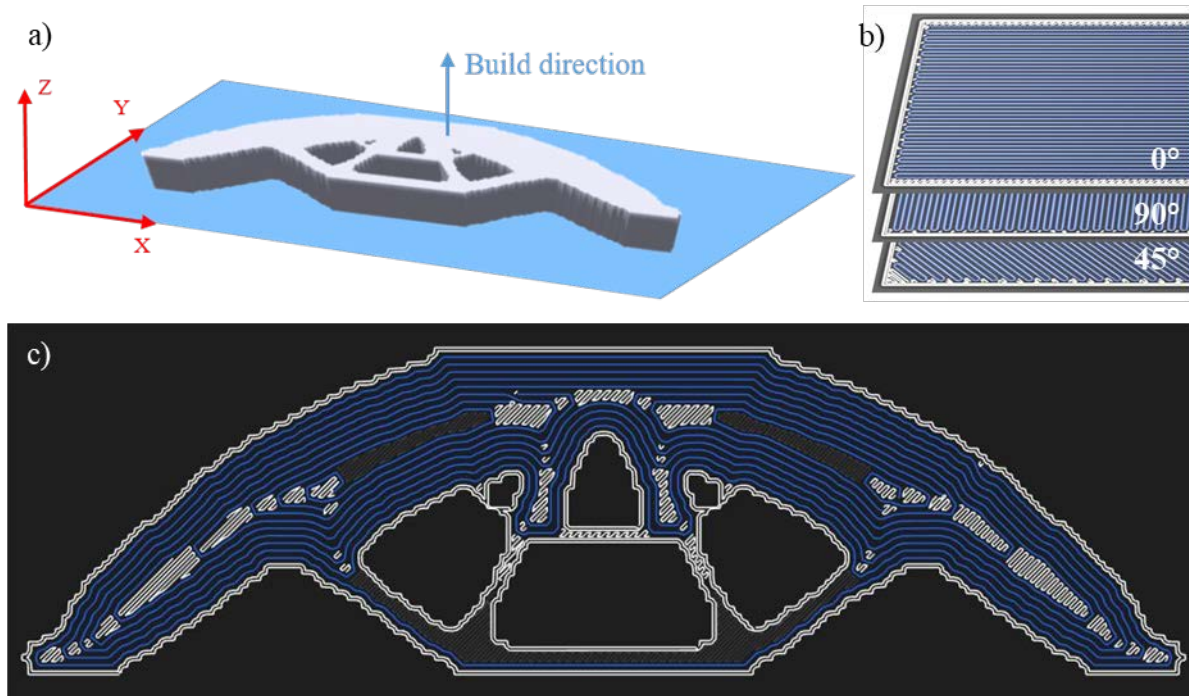


Figure 8: a) Build direction of specimens and b/c) the fibre paths (blue lines) generated by *Eiger*® [41] within the b) reference specimen with a typical QI-layup and the c) topologically optimized solution. Note: The white lines in b/c) represent pure polymer filament paths.

#### 4 Methodology – Assessing Structural Response

##### *Experimental Assessment in Three-Point-Bending*

Three-point bending test were conducted on a 50kN Instron machine at 2mm/min following the ASTM D7264 /D7264M – 15 [33] standard. The test rig consisted of support rollers with 19mm and a loading roller with 10mm diameters. Buckling guards were mounted with a total clearance of 1mm (see Figure 9).

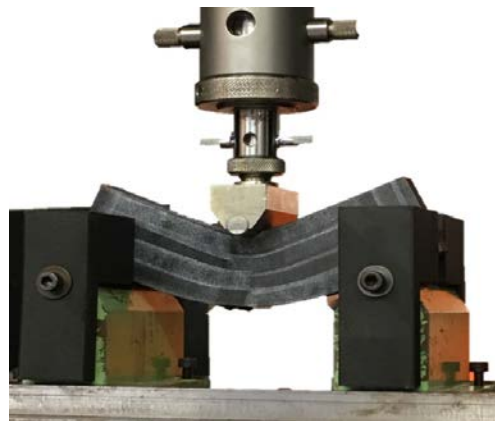


Figure 9: 3PB test setup with mounted buckling guards.

## 5 Results and Discussion

### 5.1 Numerical Investigation

**Approach I. – Isotropic topology with skeletal reinforcement.** Figure 10 displays the topologically optimized beam with the skeletal reinforcement subject to different threshold angles at a constant step size of 5 voxels. It is to note, that the iterative process of the MAT causes asymmetry in the skeleton even for a symmetric shape, as the medial axis is established from one end or branch point successively from left to right. Consequently, we observe different skeletal topologies for dissimilar threshold angles. Therefore, we have chosen an angle of  $12^\circ$  for all further analyses, which resulted in the most symmetric skeletal topology while being reasonably detailed.

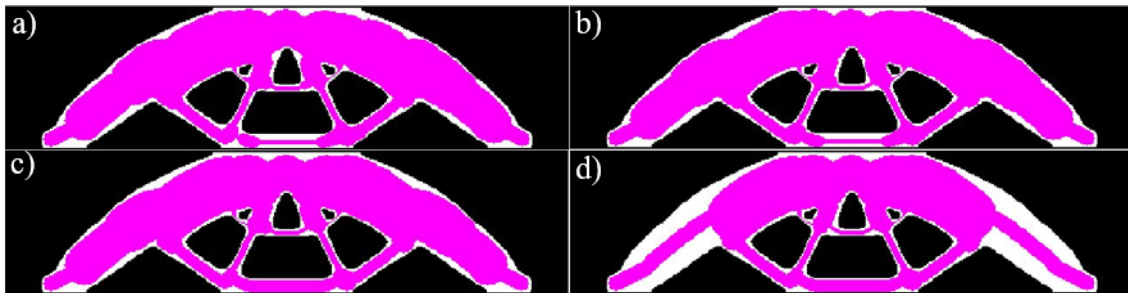


Figure 10: Dilated skeleton for threshold angles of a)  $10^\circ$ , b)  $12^\circ$ , c)  $15^\circ$  and d)  $20^\circ$ .

As expected, the structural response is non-symmetric as shown in the strain energy and strain distribution within the topology (see Figure 11 & Figure 12). Besides the loading and support points, increased strain energy can be located in the radii of the outermost branching points (also point of fracture in mechanical tests) and the horizontal strut which curves into the opposite direction compared to the loading direction. The distribution of strain along the fibre direction reveals a similar trend, since the highest values can again be located around the inner radii of the outermost branch.

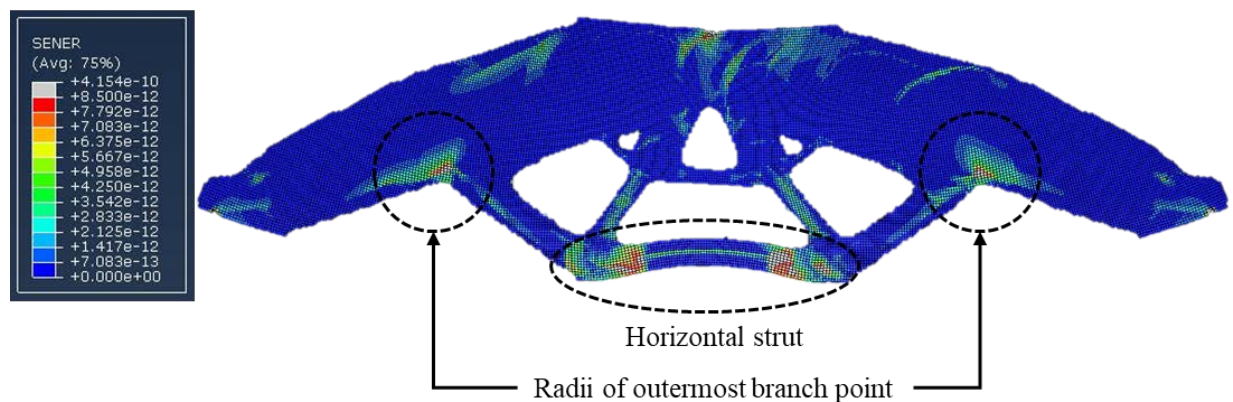


Figure 11: Strain energy distribution in the topology optimized beam with skeletal reinforcement.

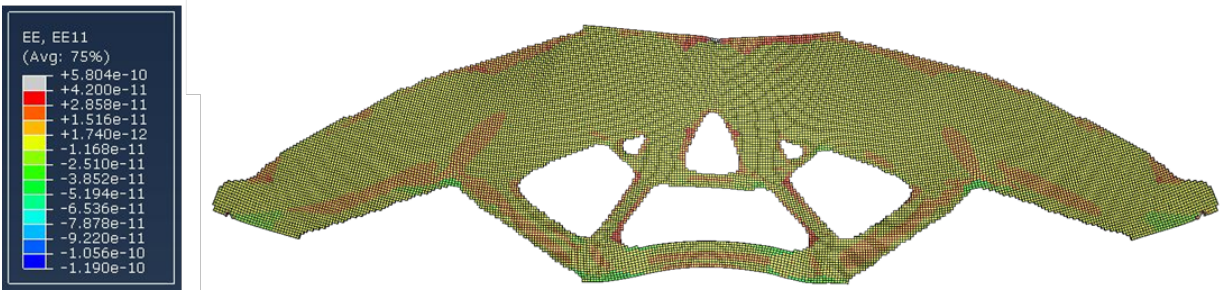


Figure 12: Strain distribution in the topology optimized beam with skeletal reinforcement in fibre direction (EE11 aligned with fibre direction).

These preliminary results highlight the need for robustly dealing with MAT information. Moreover, this might also include the requirement for a more homogenous update scheme of the fibre angles for overlapping region of the skeleton, such as a vector sum between multiple angles of neighbouring areas.

**Approach II. – Truss-like structure based on MAT.** A discretization of the skeleton with a step size of 6 and a threshold angle of  $30^\circ$  was conducted to obtain the medial axis. The nodal size optimization within the range of 1 to 3 (increments of 0.5) and the subsequent nodal perturbation yields the following trusses illustrated in Figure 13. The analyses of this particular example shows that size optimization alone results in a lower performance compared to the pure TO solution (decrease in strain energy over area from 2.25 to 1.86), however improved results were obtained with the subsequent nodal perturbation (performance increase from 1.86 to 3.23).

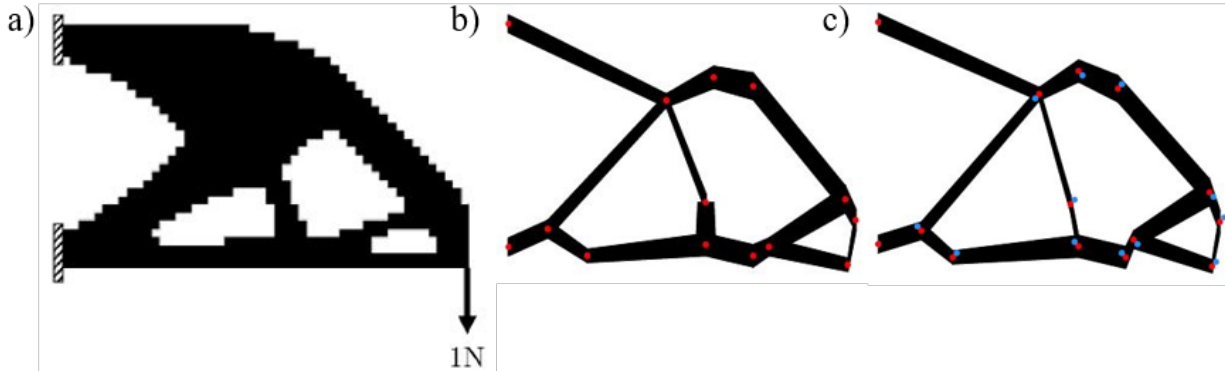


Figure 13: a) Topologically optimized cantilever and the corresponding skeleton with b) optimized nodal size and c) optimized size and location (perturbation) of nodes.

An advantage of converting the topology into a truss structure is the immediate retrieval of information on whether support is needed for AM. A limiting factor in the comparison between the topology and the truss structure is the performance measure which should be changed to a mass constraint when using anisotropic materials. Moreover, a more holistic approach i.e. a simultaneous nodal size optimization and perturbation could potentially lead to a more optimal result.

## 5.2 Experimental Investigation

**Approach I. – Isotropic topology with skeletal reinforcement.** The experimental data obtained in the 3PB test is illustrated in the form of a stress-strain curve in Figure 12. The data was collected from the load-displacement curve and calculated based on the standard [33]. Optical strain gauges would not allow the same degree of comparability as dissimilar reference points for the strain measurement would be required due to the difference in topology between reference and optimized structure. Due to the excessive local indentation, the data was analysed only after a load of 20 N, to obtain more accurate data for the global stiffness. As expected, the stress-strain curves visually displays higher flexural stiffness values of the reinforced and the reference specimens over the unreinforced and topology optimized pendants, respectively. The flexural stiffness-to-weight ratio for pure nylon and short fibre reinforced nylon favours the reference specimens (see Figure 15).

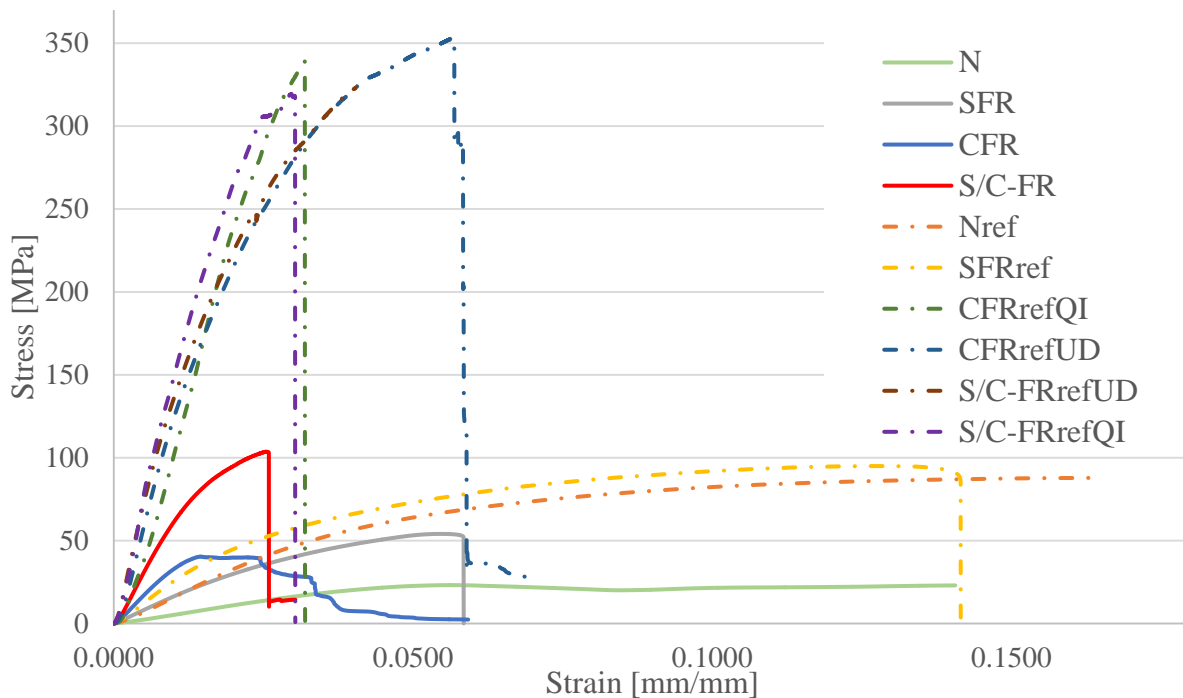


Figure 14: Stress-strain curve for the topologically optimized and reference specimens with different reinforcement types (Note that the maximum stress for the S/C-FRrefUD could not be obtained).

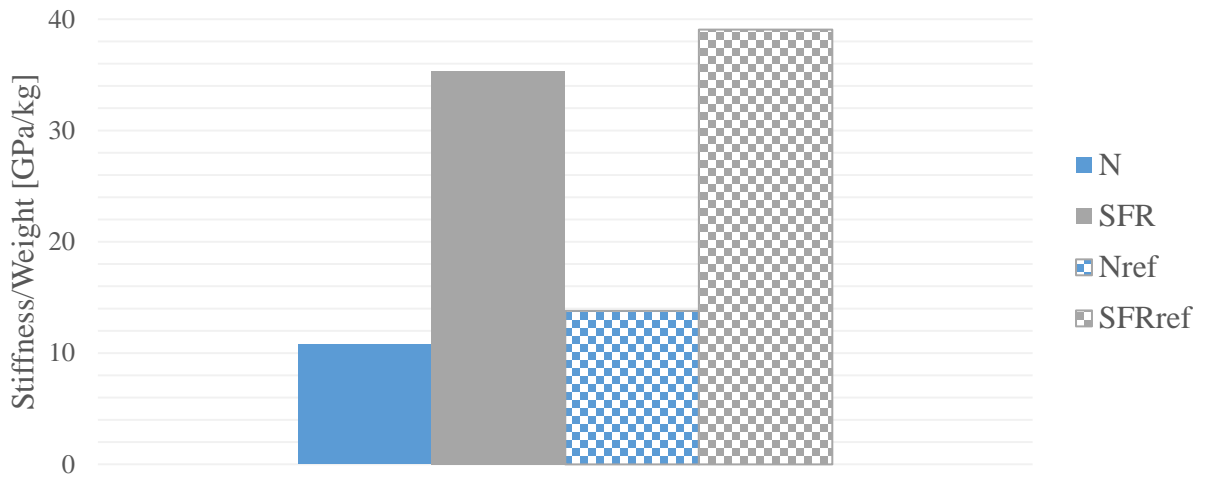


Figure 15: Flexural stiffness-to-weight ratio for the unreinforced and short fibre reinforced specimens.

Figure 16 summarize the strength and flexural stiffness values for the TO specimens tested. The continuous fibre reinforcement leads to greater flexural stiffness compared to the short fibre reinforcement and vice versa for the strength. The combination of both reinforcements (S/C-FR) displays the highest performance of all specimens for both strength and flexural stiffness and is almost equivalent to the sum of CFR and SFR. It is believed this may be due to the increased fibre volume fraction.

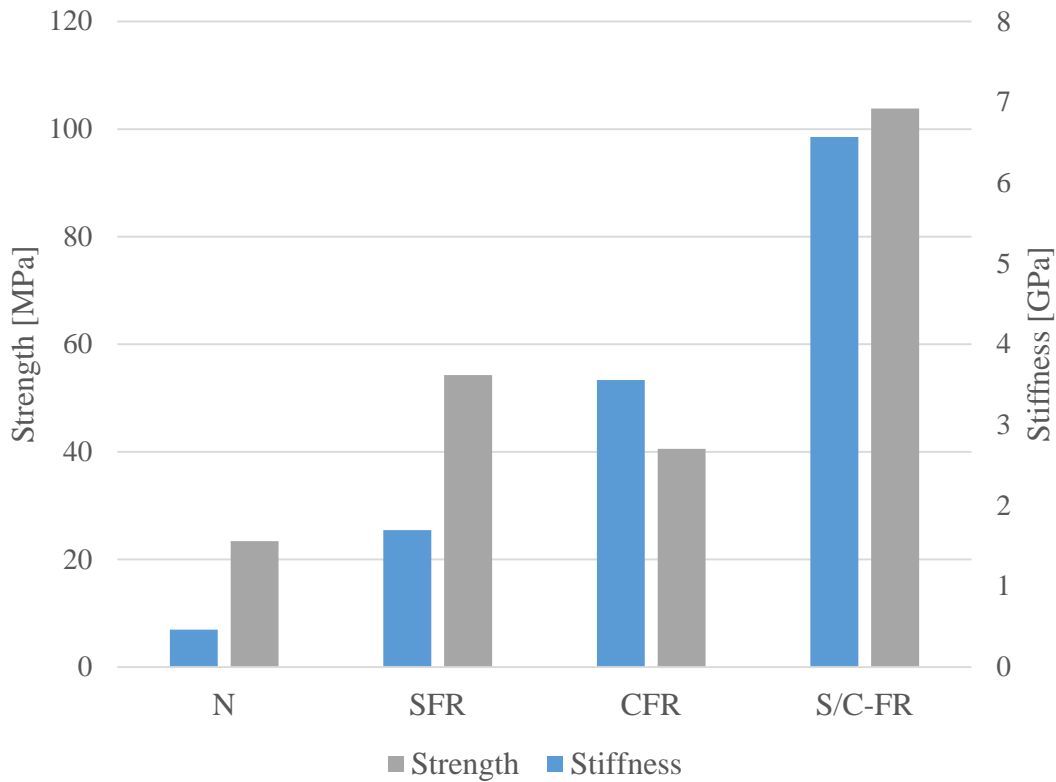


Figure 16: Results for flexural strength and stiffness of the topologically optimized specimens.

A similar trend was found in the reference specimens (see Figure 17), whereby UD specimens demonstrate a higher flexural stiffness compared to the QI specimens. The difference however becomes smaller in the specimens with additional short fibre reinforcement. Conversely to the TO specimens, the sum of each strength and stiffness values of CFRref and SFRref does not equate to the performance of S/C-FRref, in fact the strength stays pretty much constant and the flexural stiffness exceeds the sum of both constituents. The extent to which the CFRref and S/C-FRref specimens vary is unexpected, since the only difference is restricted to the minor change of the wall layers of the specimen from pure nylon to short fibre reinforced nylon. This could be attributed to testing anomalies but requires further investigation.

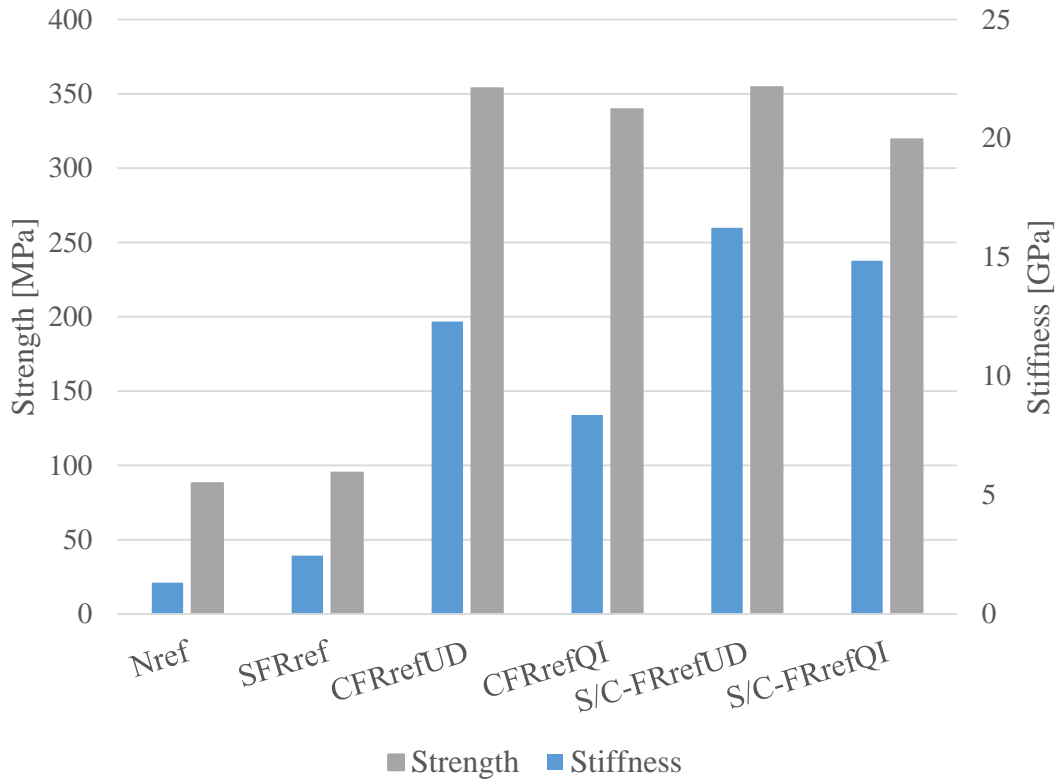


Figure 17: Results for flexural strength and stiffness of the reference specimens.

For the specimens with continuous fibre reinforcement, we chose to introduce a performance index, which represent the flexural stiffness over the fibre content (ratio between the polymer volume and the fibre volume) utilized for manufacturing. The latter was obtained by the *Eiger*® software [42]. Results show, that the topologically optimized structure performs slightly inferior to the UD reference specimens but significantly better compared to the QI reference specimen. The former is to be expected, as the UD reference specimen represent the optimal reinforcement for the maximum flexural stiffness, whereas the latter indicates that the geometrical change through TO has improved the performance, since the variation of fibre angle in the topologically optimized structure resembles that of a QI layup. Furthermore, it indicates that the placement of fibre based on the slopes of the skeletal links has been effective. This can be attributed to the fibre orientations aligned with the principle stresses.

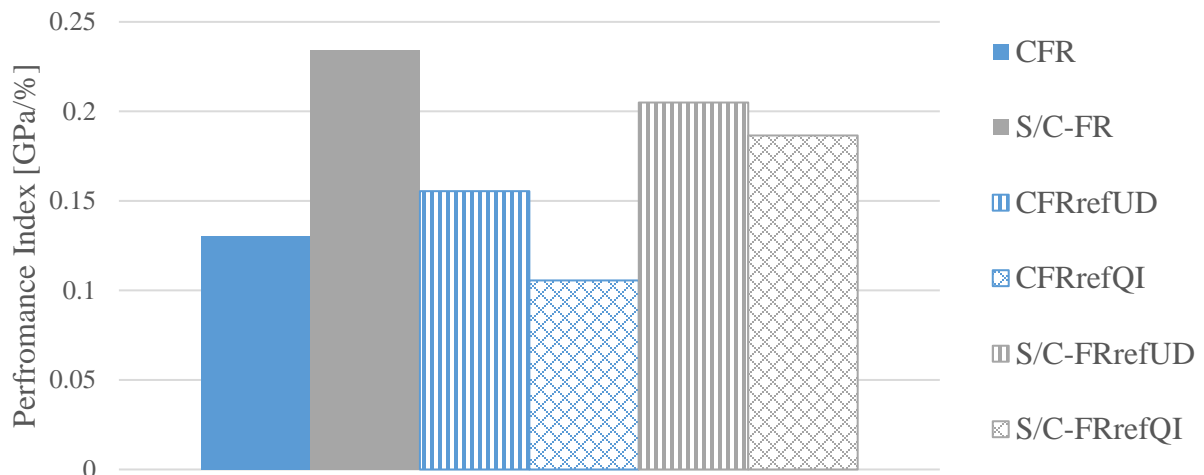


Figure 18: Performance indices (Stiffness over fibre content) for continuous fibre reinforced specimens.

## 6 Conclusion

This work has outlined approaches on how to realize light and structurally optimized designs with anisotropic considerations for AM using TO and MAT. By postprocessing the MAT information, we have demonstrated a feasible way to create a skeletal domain within an isotropic topology and an optimized truss structure from the medial axis. For the former approach we have proposed to fill the skeletal domain with continuous fibre reinforcement based on the slopes of the links to effectively improve the stiffness, as fibres are naturally placed in the direction of principle stresses. The mechanical tests, with specimens that closely resemble the proposed approach of superimposing such a skeletal reinforcement onto an isotropic topology has resulted in improved specific stiffness while reducing the weight compared to reference specimen with QI layup. We believe that the combination of C-FRAM and TO can be an effective way to create lightweight and end-use parts. Future works will therefore explore ways into realizing MAT-derived truss-like structures with anisotropic material and update schemes which would allow for an iterative change of topology at every stage based on the MAT information. Control over fibre placement and subsequently DfAM will play a key role in a successful implementation and even more efficient structures. Overcoming current limitations in software and hardware related to the tailored fibre path steering will therefore play an important role.

## 7 References

- [1] Innovative, tool-less manufacturing of complex and lightweight components, EOS GmbH

- Electro Optical Systems. (n.d.). <https://www.eos.info/automotive> (accessed February 16, 2018).
- [2] H.E. Friedrich, E. Beeh, C.S. Roeder, Solutions for Next Generation Automotive Lightweight Concepts Based on Material Selection and Functional Integration, in: D. Orlov, V. Joshi, K.N. Solanki, N.R. Neelameggham (Eds.), *Magnesium Technology 2018*, Springer International Publishing, Cham, 2018: pp. 343–348.
- [3] M. Delogu, L. Zanchi, C.A. Dattilo, M. Pierini, Innovative composites and hybrid materials for electric vehicles lightweight design in a sustainability perspective, *Materials Today Communications*. 13 (2017) 192–209. doi:10.1016/j.mtcomm.2017.09.012.
- [4] D.W. Rosen, Design for Additive Manufacturing: A Method to Explore Unexplored Regions of the Design Space, in: *7th Solid Freeform Fabrication Symposium, Texas, 2007*: pp. 402–415.
- [5] M. Kumke, H. Watschke, T. Vietor, A new methodological framework for design for additive manufacturing, *Virtual and Physical Prototyping*. 11 (2016) 3–19. doi:10.1080/17452759.2016.1139377.
- [6] D. Ding, Z. Pan, D. Cuiuri, H. Li, S. Van Duin, N. Larkin, Bead modelling and implementation of adaptive MAT path in wire and arc additive manufacturing, *Robotics and Computer-Integrated Manufacturing*. 39 (2016) 32–42. doi:10.1016/j.rcim.2015.12.004.
- [7] D. Ding, Z. Pan, D. Cuiuri, H. Li, A practical path planning methodology for wire and arc additive manufacturing of thin-walled structures, *Robotics and Computer-Integrated Manufacturing*. 34 (2015) 8–19. doi:10.1016/j.rcim.2015.01.003.
- [8] A. Panesar, D. Brackett, I. Ashcroft, R. Wildman, R. Hague, Design framework for multifunctional additive manufacturing: placement and routing of three-dimensional printed circuit volumes, *Journal of Mechanical Design – An Additive Manufacturing Special Issue*. 137 (11) (2015) 111414/1-111414/10. doi:10.1115/1.4030996.
- [9] W. Zhang, Y. Liu, P. Wei, Y. Zhu, X. Guo, Explicit control of structural complexity in topology optimization, *Computer Methods in Applied Mechanics and Engineering*. 324 (2017) 149–169. doi:10.1016/j.cma.2017.05.026.
- [10] J. Liu, A.C. To, Deposition path planning-integrated structural topology optimization for 3D additive manufacturing subject to self-support constraint, *CAD Computer Aided Design*. 91 (2017) 27–45. doi:10.1016/j.cad.2017.05.003.
- [11] A. Panesar, I. Ashcroft, D. Brackett, R. Wildman, R. Hague, Design framework for multifunctional additive manufacturing: Coupled optimization strategy for structures with embedded functional systems, *Additive Manufacturing*. 16 (2017) 98–106. doi:10.1016/j.addma.2017.05.009.

- [12] S. Liu, Y. Li, N. Li, A novel free-hanging 3D printing method for continuous carbon fiber reinforced thermoplastic lattice truss core structures, *Materials and Design*. 137 (2018) 235–244. doi:10.1016/j.matdes.2017.10.007.
- [13] P. Zhuo, S. Li, I. Ashcroft, A. Jones, J. Pu, 3D Printing of Continuous Fibre Reinforced Thermoplastic Composites, in: 21st International Conference on Composite Materials, 2017.
- [14] L.G. Blok, B.K.S. Woods, H. Yu, M.L. Longana, K.P. Potter, 3D Printed Composites – Benchmarking the state of the art, in: 21st International Conference on Composite Materials, 2017.
- [15] A.N. Dickson, J.N. Barry, K.A. McDonnell, D.P. Dowling, Fabrication of continuous carbon, glass and Kevlar fibre reinforced polymer composites using additive manufacturing, *Additive Manufacturing*. 16 (2017) 146–152. doi:10.1016/j.addma.2017.06.004.
- [16] B.G. Compton, J.A. Lewis, 3D-printing of lightweight cellular composites, *Advanced Materials*. 26 (34) (2014) 5930–5935. doi:10.1002/adma.201401804.
- [17] M. Ivey, G.W. Melenka, J.P. Carey, C. Ayranci, Characterizing short-fiber-reinforced composites produced using additive manufacturing, *Advanced Manufacturing: Polymer & Composites Science*. 0340 (2017) 1–11. doi:10.1080/20550340.2017.1341125.
- [18] J.J. Martin, B.E. Fiore, R.M. Erb, Designing bioinspired composite reinforcement architectures via 3D magnetic printing, *Nature Communications*. 6 (2015) 1–7. doi:10.1038/ncomms9641.
- [19] L.R. Holmes, J.C. Riddick, Research summary of an additive manufacturing technology for the fabrication of 3D composites with tailored internal structure, *Jom*. 66 (2014) 270–274. doi:10.1007/s11837-013-0828-4.
- [20] S. Christ, M. Schnabel, E. Vorndran, J. Groll, U. Gbureck, Fiber reinforcement during 3D printing, *Materials Letters*. 139 (2015) 165–168. doi:10.1016/j.matlet.2014.10.065.
- [21] Z. Quan, A. Wu, M. Keefe, X. Qin, J. Yu, J. Suhr, J.H. Byun, B.S. Kim, T.W. Chou, Additive manufacturing of multi-directional preforms for composites: Opportunities and challenges, *Materials Today*. 18 (2015) 503–512. doi:10.1016/j.mattod.2015.05.001.
- [22] Composite 3D Printing, Markforged, Inc. (2017). <https://markforged.com/composites/> (accessed December 14, 2017).
- [23] The revolution will be printed™, Arevo Inc. (2017). <http://arevolabs.com/> (accessed December 14, 2017).
- [24] Continuous Fiber 3D Printing, Continuous Composites. (2017). <http://continuouscomposites.com/> (accessed December 14, 2017).

- [25] Y. Wang, Z. Kang, A level set method for shape and topology optimization of coated structures, *Computer Methods in Applied Mechanics and Engineering*. 329 (2018) 553–574. doi:10.1016/j.cma.2014.01.014.
- [26] Y. Wang, Z. Luo, Z. Kang, N. Zhang, A multi-material level set-based topology and shape optimization method, *Computer Methods in Applied Mechanics and Engineering*. 283 (2015) 1570–1586. doi:10.1016/j.cma.2014.11.002.
- [27] B. Zhu, M. Skouras, D. Chen, W. Matusik, Two-Scale Topology Optimization with Microstructures, *ACM Transactions on Graphics*. 36 (2017) 1–16. doi:10.1145/3095815.
- [28] L.G.B. Jácome, B.F. Tating, R. Harik, Z. Gürdal, A.A.W. Blom-Schieber, M. Rassaian, S. Wanthal, An analysis framework for topology optimization of 3D printed reinforced composites, *AIAA/ASCE/AHS/ASC Structures, Structural Dynamics, and Materials Conference*, 2018. (2018) 1–15. doi:10.2514/6.2018-0093.
- [29] R. Høglund, D.E. Smith, Non-Isotropic Material Distribution Topology Optimization for Fused Deposition Modeling Products, in: *Proceeding of the 2015 Solid Freeform Fabrication Symposium*, Austin, TX., 2015: pp. 888–903. doi:10.1017/CBO9781107415324.004.
- [30] D. Jiang, D.E. Smith, Predicting Short Fiber Composite Material Distribution and Orientation Using Optimization for Additive Manufacturing Applications, in: *SPE ANTEC® Anaheim 2017*, 2017: pp. 94–99.
- [31] D. Jiang, D.E. Smith, Topology Optimization For 3D Material Distribution And Orientation In Additive Manufacturing, in: *Solid Freeform Fabrication*, 2017: pp. 2236–2249.
- [32] R. Høglund, D.E. Smith, Continuous Fiber Angle Topology Optimization for Polymer Fused Filament Fabrication, in: *Solid Freeform Fabrication Symposium*, 2016: pp. 1078–1090.
- [33] ASTM, Standard Test Method for Flexural Properties of Polymer Matrix Composite Materials 1, *Annual Book of ASTM Standards*. (2010) 1–11. doi:10.1520/D7264.
- [34] O. Sigmund, A 99 line topology optimization code written in Matlab, *Structural and Multidisciplinary Optimization*. 21 (2001) 120–127. doi:10.1007/s001580050176.
- [35] E. Andreassen, A. Clausen, M. Schevenels, B.S. Lazarov, O. Sigmund, Efficient topology optimization in MATLAB using 88 lines of code, *Structural and Multidisciplinary Optimization*. 43 (2011) 1–16. doi:10.1007/s00158-010-0594-7.
- [36] K. Liu, A. Tovar, An efficient 3D topology optimization code written in Matlab, *Structural and Multidisciplinary Optimization*. 50 (2014) 1175–1196. doi:10.1007/s00158-014-1107-x.

- [37] M. Kerschnitzki, P. Kollmannsberger, M. Burghammer, G.N. Duda, R. Weinkamer, W. Wagermaier, P. Fratzl, Architecture of the osteocyte network correlates with bone material quality, *Journal of Bone and Mineral Research*. 28 (2013) 1837–1845. doi:10.1002/jbmr.1927.
- [38] MathWorks.Matlab. (Version R2018a) [Software] MathWorks Inc., (2018). [https://uk.mathworks.com/products/new\\_products/latest\\_features.html](https://uk.mathworks.com/products/new_products/latest_features.html) (accessed July 2, 2018).
- [39] Dassault Systèmes (2016) Abaqus CAE [Software] Dassault Systèmes, (n.d.). <https://www.3ds.com/products-services/simulia/products/abaqus/abaquscae/> (accessed July 3, 2018).
- [40] Material Specifications - Composites, Markforged, Inc. (2018). [https://static.markforged.com/markforged\\_composites\\_datasheet.pdf](https://static.markforged.com/markforged_composites_datasheet.pdf) (accessed June 17, 2018).
- [41] Markforged (2018) Eiger (Version 4db22ab) [Software] Markforged Inc, (n.d.). <https://markforged.com/eiger/> (accessed July 3, 2018).
- [42] Markforged (2018) Eiger (Version 4db22ab) [Software] Markforged Inc, (n.d.).